ACS APPLIED MATERIALS & INTERFACES

Research Article

www.acsami.org

Improving the Efficiency of ZnO-Based Organic Solar Cell by Self-Assembled Monolayer Assisted Modulation on the Properties of ZnO Acceptor Layer

Jian-Ming Chiu and Yian Tai*

Department of Chemical Engineering, National Taiwan University of Science and Technology, Taipei, Taiwan

Supporting Information

ABSTRACT: In this study, we fabricated a bilayer hybrid organic solar cell with P3HT as the donor and ZnO as the acceptor (ITO/ZnO/P3HT/Au). We show that passivating a self-assembled monolayer (SAM) over the ITO electrode surface before fabricating the ZnO layer improves the crystallinity of the ZnO layer and of the P3HT layer spin-coated on top of the ZnO layer. The SAM modification resulted in improved charge mobility in the ZnO and P3HT layers. As a consequence, the short circuit current of the photovoltaic device were enhanced. The power conversion efficiency of the SAM-modified device was approximately 60% higher than that of the untreated device. Our findings suggest that the performance of metal oxide-based organic solar cells can be improved by SAM-assisted modulation of metal oxide crystallinity.

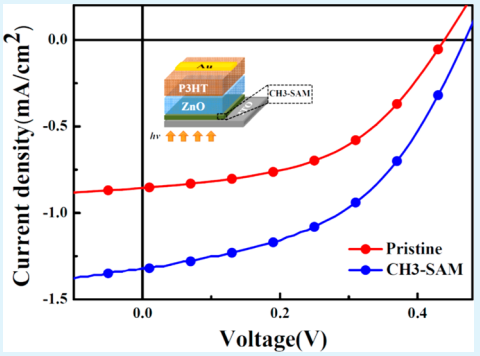

KEYWORDS: *polymer, ZnO, solar cells, self-assembled monolayer, crystallinity*

INTRODUCTION

Polymer/metal oxide heterojunction or hybrid photovoltaic devices (hybrid solar cells, HSCs) have attracted considerable attention recently because these devices are scalable, can be manufactured inexpensively, and can be processed in solution at low temperatures.[1] However, the power-conversion efficiency (PCE, η) of current HSCs is extremely low because of factors, such as the incompatibility of the interface between organic and inorganic materials or the low charge mobility of the metal oxide resulting from its low crystallinity. Methods to improve the performance of hybrid photovoltaic devices have so far focused mainly on the interfaces between inorganic and organic materials, and several studies have reported improving the interfaces.[2−4] Two main approaches have been applied for the interfacial modification: (1) a nanostructure electron-accepting layer was tailored to enhance the photocurrent by increasing the donor−acceptor interfacial area[5] and (2) exciton dissociation and charge transfer were increased by modifying the interfaces between metal oxides and polymers.[6] However, little effort has been devoted to improving the electrical properties of the metal oxide acceptor, because this requires enhancing metal oxide qualities, such as crystallinity using high temperatures, which is unsuitable for the ITO electrode.[7,8]

Here, we used a planar heterojunction with P3HT/ZnO (donor/acceptor) as a model system to demonstrate how bulk modification of the acceptor layer affects the performance of the HSC. We introduced a self-assembled monolayer (SAM) to improve the quality of the ZnO thin film without high-temperature treatment. Specifically, we fabricated the SAM on the ITO electrode surface and deposited ZnO as the acceptor layer on top of it.

The SAM technique, which was developed recently to improve the quality of thin films of transparent conducting oxides under ambient conditions at room temperature,[9,10] provides a unique opportunity to manipulate the physical and chemical properties of the surfaces of a variety of substrates.[11−13] As a result of the change induced in the substrate's surface properties, crystal growth on SAM-functionalized surfaces can be controlled.[14−16] Moreover, fabricating small molecular SAMs between a metal/semiconductor junction affects the intrinsic charge transport through that interface, because the electrical properties of metal/semiconductor junctions can be manipulated depending on the dipole moment of the functional group and the backbone of the SAM molecule on the substrate.[17−20]

On the basis of the above findings, we extended the concept of modifying surfaces with SAMs to the growing ZnO films on alkylsilane-functionalized ITO substrates using the spray pyrolysis method. ZnO films grown on CH3-terminated SAMs are highly crystalline compared with the ZnO deposited on pristine ITO. Therefore, the performance of HSC devices with ZnO acceptors fabricated using the SAM technique can be improved substantially, because the acceptor layer's electrical properties are enhanced by the improvement of ZnO quality.

Received: March 14, 2013
Accepted: July 12, 2013
Published: July 29, 2013

dx.doi.org/10.1021/am400928n | ACS Appl. Mater. Interfaces 2013, 5, 6946−6950

EXPERIMENTAL SECTION

Materials. All ITO (the sheet resistance of 15 Ω/□) substrates used for the deposition were purchased from Merck. *N*-Propyltriethoxysilane (CH_3-SAM, 97%, Aldrich), was used as received. The poly(3-hexylthiophene-2,5-diyl), P3HT, 99.999% was purchased from Rieke Metals (#BS19-04), and zinc acetate ($(C_2H_3O_2)Zn$), 99.99%, was used as received from the Sigma-Aldrich.

Modification of SAM. The ITO substrates were degreased by dilute detergent followed by sonication in an ultrasonic bath using different solvents in the sequence of deionized water, acetone, and 2-propanol (IPA) and finally treated with UV/ozone prior to further use. Afterward, the ITO substrates were immersed in 0.2 mM solutions of CH_3-SAM molecules in decane for 24 h. After removing it from the solutions, ITO substrates were rinsed with decane and blown dry by constant N_2 flow.

Device Fabrication. ZnO films were prepared using spray pyrolysis method. The detailed procedure is described in Supporting Information (SI). Afterward, we carried out SEM measurements to determine the thickness of the films. From SEM cross section (Figure S2 in SI), the thickness of pristine and SAM-modified ZnO films were 85 and 80 nm, respectively. For the fabrication of ZnO/P3HT HSC device, ∼75 nm P3HT were spin-coated from a 30 mg/mL chlorobenzene solution on top of the ZnO layers. Finally, 60 nm Au top contacts were deposited via thermal evaporation through a shadow mask with active areas for each device of 0.063 cm^2. Afterward, the whole device was annealed at 150 °C for 20 min.

Characterization. Current voltage (*J*−*V*) characteristics of the devices were obtained via an *I*−*V* source meter (Keithley 2400) under a dark condition and the illumination of an AM 1.5 G irradiation at 100 mW cm^{-2} using xenon-lamp based solar simulator (Newport-Oriel 500 W Solar Simulator). An aperture with the size of 2 mm × 2 mm was applied on the HSC to confine the active area of our devices. External quantum efficiency (EQE) was determined using a 300 W Xe lamp-based solar simulator (Oriel arc lamp #66160). The electrical properties were measured using Ecopia HMS-3000 Hall measurement and the crystallinities were investigated by subjecting the samples to X-ray diffraction (XRD, PANalyticalX'Pert PRO). The surface morphology of the device was probed using an atomic force microscope (AFM; Digital Nanoscope III A) operating in tapping mode.

RESULTS AND DISCUSSION

The pristine (unmodified) and CH_3-SAM-modified ITO electrode surfaces were characterized by measuring contact angles (CAs) (Figure 1). Without SAM modification, the ITO surface after UV/ozone treatment had a low wetting angle to DI water (approximately 5°), suggesting that the ITO surface was hydrophilic. However, the CA increased drastically, to nearly 90°, after modifying the surface with SAMs. From the CA results, we confirmed that alkylsilane SAM was fabricated successfully on the ITO electrode.[21−23] The surface energies of pristine and SAM-modified ITO substrates were deduced from CAs using the Zisman plot[24] as 74.4 and 26.1 mN/m, respectively.

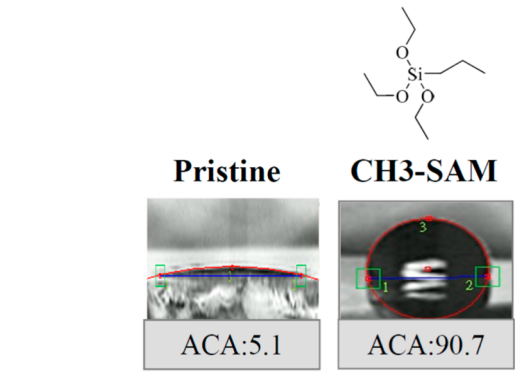

	Pristine	CH3-SAM
γ (mNm^{-1})	74.4±1.3	26.1±2.6

Figure 1. Water contact angles and surface energies of pristine and CH_3-SAM-modified ITO surfaces.

To fabricate the ZnO acceptor layer on pristine and SAM-modified ITOs, we used the spray pyrolysis method, with a process temperature of 280 °C. To confirm that the CH_3-SAM remained intact under this temperature, we performed XPS and FTIR on SAM/ITO at several annealing temperatures, and the results are shown in Figure S3 in SI. Because the SAM molecules were composed of alkyl chains with silane functional groups, the configuration of SAM on ITO could be examined by monitoring the changes in C1s and Si2p signals with changing substrate temperatures. The spectra shown in SI Figure S3a and S3b verified that CH_3-SAM can be maintained on the substrate even at 350 °C annealing temperature; the C1s and Si2p signals were identical at various annealing temperatures. Moreover, the IR fingerprint of $-CH_3$ vibration, absorption peaks at 2800−3000 cm^{-1}, were observed for SAMs at room temperature and after annealing at 350 °C with only minor changes in the profile,[25] as shown in SI Figure S3c. Therefore, from the XPS and FTIR results, we concluded that the 280 °C process temperature did not damage the SAMs.

Surfaces of both the pristine and SAM-modified substrates (ITO and ZnO/ITO) were characterized using atomic force microscopy (AFM) (Figure 2). The pristine ITO (Figure 2a) and the ZnO layer fabricated on the ITO substrate (Figure 2b) showed greater surface roughness (2.2 and 2.7 nm, respectively) than SAM-modified ITO (Figure 2c) and ZnO/SAM-modified ITO (1.7 and 2.1 nm, respectively; Figure 2d). SAMs are known to cover the defects of a substrate and reduce surface roughness,[26−28] which explains why the ZnO film fabricated on SAM-modified ITO was smoother than the film fabricated on pristine ITO.

Next, we fabricated the HSC device, the architecture of which is shown in the inset of Figure 3. The current density−voltage (*I*−*V*) characteristics of the pristine and SAM-modified solar cells are plotted in Figure 3, and the device parameters and the average performances are summarized in Table 1. The PCE of pristine HSC was 0.18%, with a short-circuit current (J_{sc}) of 0.85 mA/cm^2 and an open-circuit voltage (V_{oc}) of 0.44 V. In contrast, the CH_3-SAM-modified device had a PCE of 0.29%, an improvement of approximately 60%, as well as higher J_{sc} (1.32 mA/cm^2) and Voc (0.47 V). These *I*−*V* measurements indicated that the device was superior mainly because of the large increase in J_{sc}. To investigate how J_{sc} was enhanced, we compared the device characteristics of pristine and SAM-modified HSC by showing the external quantum efficiency (EQE) of the devices is presented in Figure 4. Across the entire spectrum, EQE for the CH_3-SAM modified cell was evidently improved compare to the EQE for pristine HSC. By integrating the EQE spectra, we calculated the J_{sc} values, which are presented in the table in Figure 4 alongside J_{sc} values measured from *I*−*V* curves. The J_{sc} values calculated from EQE match the measured values closely (error approximately 5%), further confirming that the PCE of the CH_3-SAM-modified device was improved mainly because of the substantial increase in J_{sc}. We also present the UV−vis absorption spectra and internal

dx.doi.org/10.1021/am400928n | ACS Appl. Mater. Interfaces 2013, 5, 6946−6950

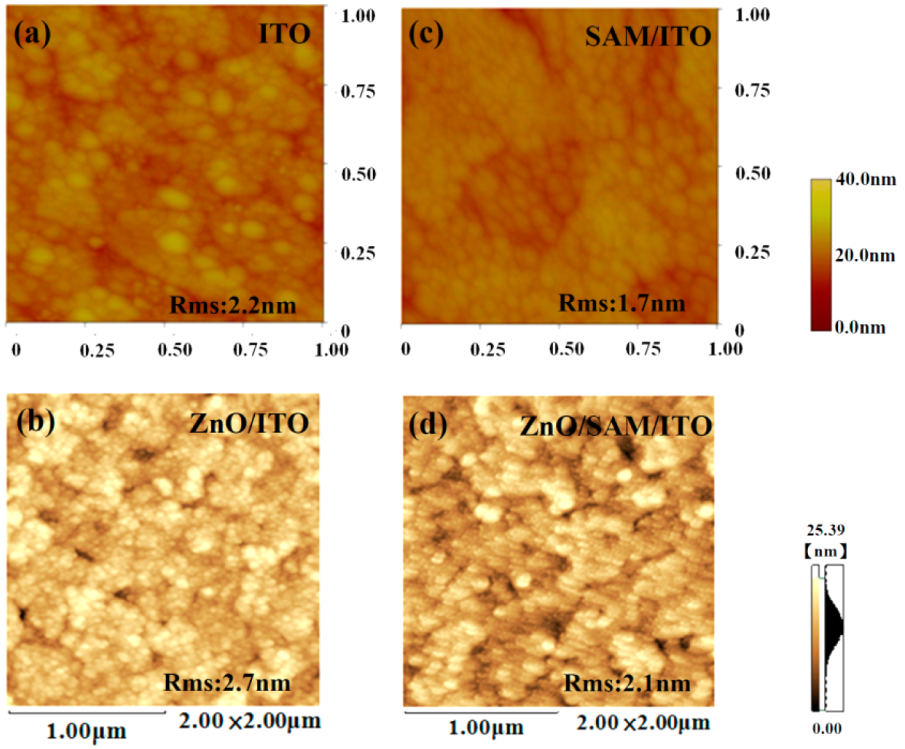

Figure 2. Tapping mode AFM images of pristine (a) and SAM-modified (c) ITO (1×1 μm^2) and ZnO fabricated on pristine (b) and SAM-modified (d) ITO (2×2 μm^2).

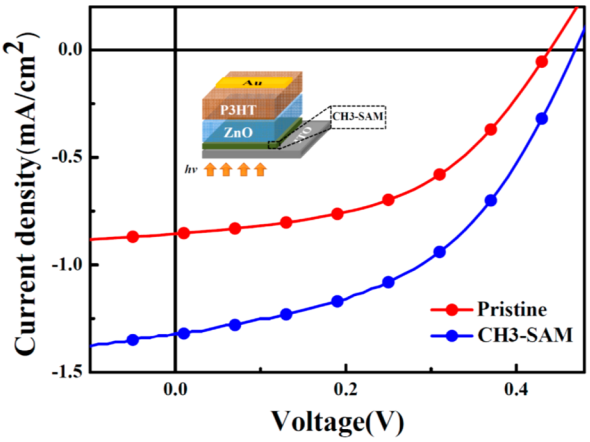

Figure 3. $J-V$ characteristics of pristine and SAM-modified HSC under simulated AM 1.5 illumination with light density of 100 mW/cm^2.

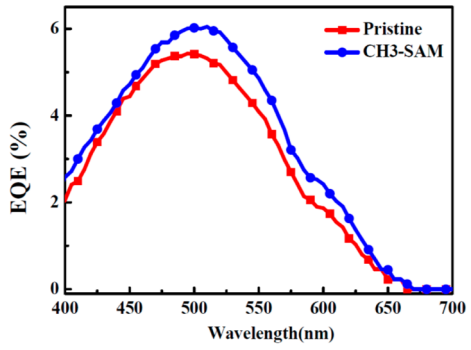

Device	Measured Jsc	Calculated Jsc	Error (%)
Pristine	0.85	0.90	5.9%
CH3-SAM	1.32	1.25	5.3%

Figure 4. External quantum efficiency (EQE) of pristine and SAM-modified HSC devices, and the J_{sc} values obtained from $I-V$ measurements and calculated from EQE results.

Table 1. Photovoltaic Parameters of the Pristine and SAM-Modified HSC Devices

device	J_{sc} (mA/cm^2)	V_{oc} (V)	η (%)	FF(%)
pristine	0.85 ± 0.05	0.44 ± 0.02	0.18 ± 0.04	48 ± 2
CH_3-SAM	1.32 ± 0.07	0.47 ± 0.03	0.29 ± 0.01	47 ± 1

quantum efficiency (IQE) profiles in Figures S4 and S5 in SI. Because the IQE results were calculated from the measured UV−vis and EQE spectra, IQE enhancement was inferred to be a result of the improvement of the electrical properties.[29] Therefore, we concluded that HSC performance was improved after SAM-modification because the electrical properties of the device had been improved. Notably, in the IQE spectrum of the SAM-modified device, a large enhancement was observed at approximately 625 nm, which merely caused by small changes at the absorption tail of P3HT.

Because SAM-modification altered only the properties of the ZnO layer, to understand the effect of SAMs on ZnO films better, we used the Van der Pauw method and $I-V$ measurements[30] to determine both the lateral and vertical electrical properties of ZnO films fabricated on unmodified and SAM-modified ITOs: lateral Hall mobilities obtained using the Van der Pauw method were 29.1 and 40.1 cm^2 V^{-1} S^{-1}, respectively; and vertical mobilities obtained from $I-V$ measurements were 4.2 and 5.0 cm^2 V^{-1} S^{-1}, respectively. Thus, the electrical properties of ZnO films varied depending on the nature of the ITO substrates. The ZnO film grown on

dx.doi.org/10.1021/am400928n | ACS Appl. Mater. Interfaces 2013, 5, 6946−6950

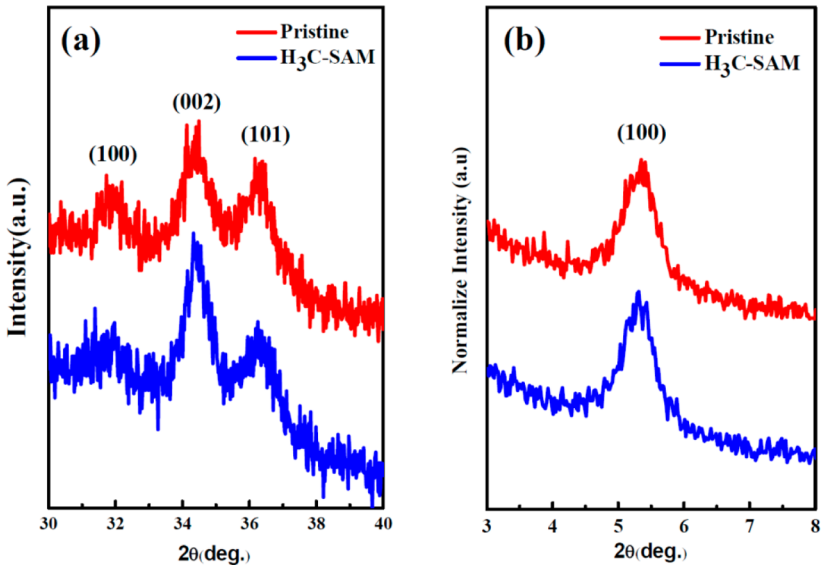

Figure 5. XRD patterns of ZnO films deposited on pristine and SAM-modified ITO (a) and P3HT layers annealed at 150 °C on ZnO fabricated on pristine and SAM-modified ITO (b).

CH_3-SAM-modified ITO substrate had higher carrier mobility in both the vertical and the lateral directions than ZnO fabricated on the pristine substrate. In principle, the electron transport properties of the pristine device (ZnO/ITO) should superior the SAM-modified device (ZnO/SAM/ITO) because the SAM backbone increases the electron transport barrier.[20] Moreover, the $-CH_3$ functional group has an insignificant dipole that contributes little to charge transfer.[19] Therefore, we concluded that the electrical properties of the SAM-modified device increased because the ZnO film property improved.

To study how SAM modification affected the crystallinity of ZnO and P3HT/ZnO, we conducted X-ray diffraction (XRD) studies. Figure 5a shows the XRD profiles of ZnO films grown on pristine and SAM-modified ITO; notably, both profiles exhibit 3 peaks corresponding to (100), (002), and (101) crystal planes. The predominant plane (002) was at approximately 34.5°, which indicates a hexagonal wurtzite structure. The full width at half-maximum (fwhm) and the normalized peak-area ratio of peak (002) for pristine and SAM-modified ZnO are shown in Table 2. The peak-area ratio of (002) was used to normalize to the summation of the peak areas of (100), (002), and (101). The XRD profiles, the fwhm values, and the peak-area ratios showed collectively that the crystallinity of ZnO fabricated on SAM-modified ITO was superior to that of ZnO film on pristine ITO. The *c*-axis (002) orientation is known to be responsible for vertical charge mobility in ZnO films.[31,32] Therefore, the XRD results confirmed that the electrical properties of the ZnO on SAM-modified ITO improved because of the improved crystallinity of the film. We suggest that ZnO crystallinity improved mainly because the ITO surface energy decreased after SAM-modification. To achieve high crystallinity in thin films deposited on foreign substrates, the surface energy of the substrate must be compensated for to increase the atomic mobilities of the deposited species on the substrate surface.[33] Because CH_3-SAM reduced the surface energy of the ITO substrate, the deposited species (Zn and O) might have sufficient mobilites on CH_3-modified ITO surfaces to account for the superior crystallinity of the ZnO film.

Table 2. Summary of the Crystallinity Properties of ZnO Films Fabricated on Pristine and SAM-Modified ITO Surfaces and P3HT Layers on the Corresponding ZnO Films

sample	ZnO (002) peak area ratio[a]	ZnO(002) fwhm	P3HT(100) fwhm
pristine	47%	0.63°	0.61°
CH_3-SAM	56%	0.47°	0.51°

[a]The ZnO (002) peak area ratio was normalized to the summation peak areas of (100), (002), and (101).

Moreover, the XRD spectra in Figure 5b and the fwhm in Table 2 of P3HT on ZnO film showed similar results. The SAM-modified film (P3HT/ZnO/CH_3-SAM/ITO) showed a narrower fwhm in the P3HT peak (100) than the film on ZnO/ITO, suggesting a superior crystallinity of the P3HT film on ZnO/SAM/ITO. The crystallinity of the P3HT film, which depends on the polymer/substrate interaction, is known to affect the film's electrical properties.[34] This was confirmed further by the UV−vis absorption results shown in Supporting Information Figure S4. The absorption peak between 600 and 620 nm, originating from the $\pi-\pi^*$ optical transition of P3HT, was slightly larger for P3HT on ZnO/SAM/glass than for P3HT on pristine ZnO film, which suggested that the P3HT polymeric chains conjugate better and form nanodomains on ZnO/SAM/glass.[35,36] As a consequence, better charge transfer can be expected within P3HT film on ZnO/SAM/ITO.

The results of XRD, Hall measurements, and *I*−*V* measurements confirmed that the photocurrent in the SAM-modified HSC device was enhanced because of the improved crystallinity of the ZnO layer, which led to higher charge mobility in the acceptor layer and to the enhanced crystallinity of P3HT, which improved the electrical properties of the donor layer. Therefore, better charge transfer can be expected in both ZnO and P3HT.

The V_{oc} of the SAM-modified device was slightly higher than that of the pristine HSC. Using AFM, the surface roughness of P3HT on ZnO was measured at approximately 4.5 nm for pristine film and approximately 3.5 nm for CH_3-SAM-modified film. Changes in the morphological properties of P3HT are

known to change the V_{oc}.[37,38] Therefore, the improved morphology of P3HT after SAM modification might have increased the V_{oc}, although this is not conclusive as the changes in V_{oc} and the surface morphology of P3HT were small.

CONCLUSION

In conclusion, we have demonstrated a simple and effective approach to improve the performance of a ZnO-based HSC device. SAM modification affected crystal growth of the ZnO thin film markedly. The crystallinity, surface morphology, and the surface work function of the ZnO film were improved after SAM modification under mild conditions, which also improved the crystallinity of the P3HT layer on top of the ZnO thin film. Using this method, the electrical properties of both the donor and acceptor layers can be enhanced and, as a result, the J_{sc}, Voc, and PCE of the solar cell can be improved considerably. Therefore, our study provides a technique for improving the electrical properties of an inorganic layer in a device without heating, an approach that could be applied widely in organic hybrid device fabrication processes that are vulnerable to high temperatures.

ASSOCIATED CONTENT

Supporting Information

Detailed procedure for the fabrication of ZnO thin film with spray pyrolysis method, SEM cross-section images of ZnO thin film fabricated on pristine ITO and CH_3-SAM-modified ITO, XPS, and FTIR spectra of CH_3-SAM on ITO featuring different substrate annealing temperatures, and UV−vis absorption spectra and IQE spectra of pristine and SAM-modified HSC devices. This material is available free of charge via the Internet at http://pubs.acs.org.

AUTHOR INFORMATION

Corresponding Author

*Address: Department of Chemical Engineering, National Taiwan University of Science and Technology, 43 Keelung Road Sec. 4, Taipei106, Taiwan. Phone: +886-2-2737-6620. Fax: +886-2-2737-6644. E-mail: ytai@mail.ntust.edu.tw.

Notes

The authors declare no competing financial interest.

ACKNOWLEDGMENTS

The authors are grateful to Prof. Kuei-Hsian Chen and Prof. Li-Chyong Chen for their constant support on this project, and Prof. Thomas C. K. Yang of NTUT for the support of XRD instrumentation. This work was financially supported by Academia Sinica and NTUST.

REFERENCES

(1) Olson, D. C.; Piris, J.; Collins, R. T.; Shaheen, S. E.; Ginley, D. S. *Thin Solid Films* **2006**, *496*, 26−29.
(2) Monson, T. C.; Lloyd, M. T.; Olson, D. C.; Lee, Y.−J.; Hsu, J. W. P. *Adv. Mater.* **2008**, *20*, 4755−4759.
(3) Vaynzof, Y.; Kabra, D.; Zhao, L.; Ho, P. K. H.; Wee, A. T.-S.; Friend, R. H. *Appl. Phys. Lett.* **2010**, *97*, 033309−033311.
(4) Allen, C. G.; Baker, D. J.; Brenner, T. M.; Weigand, C. C.; Albin, J. M.; Steirer, K. X.; Olson, D. C.; Ladam, C.; Ginley, D. S.; Collins, R. T.; Furtak, T. E. *J. Phys. Chem. C.* **2012**, *116*, 8872−8880.
(5) Lee, Y. J.; Lloyd, M. T.; Olson, D. C.; Grubbs, R. K.; Lu, P.; Davis, R. J.; Voigt, J. A.; Hsu, J. W. P. *J. Phys. Chem. C.* **2009**, *113*, 15778−15782.
(6) Lloyd, M. T.; Prasankumar, R. P.; Sinclair, M. B.; Mayer, A. C.; Olson, D. C.; Hsu, J. W. P. *J. Mater. Chem.* **2009**, *19*, 4609−4614.
(7) Giefers, H.; Porsch, F.; Wortmann, G. *Solid State Ionics* **2005**, *176*, 199.
(8) Yıldırım, T.; Ğur, E.; T̈uzemen, S.; Bilgin, V.; K̈ose, S.; Atay, F.; Akÿuz, I. *Phys. E* **2005**, *27*, 290.
(9) Sharma, J.; Chang, H. C.; Tai, Y. *Langmuir* **2010**, *26*, 8251−8255.
(10) Aklilu, M.; Tai, Y. *Appl. Surf. Sci.* **2013**, *270*, 648−654.
(11) Ulman, A. *Chem. Rev.* **1996**, *96*, 1533−1554.
(12) Gooding, J. J.; Mearns, F.; Yang, W.; Liu, J. *Electroanalysis* **2003**, *15*, 81−96.
(13) Frank, S. *J. Phys.: Condens. Matter.* **2004**, *16*, R881.
(14) Bunker, B. C.; Rieke, P. C.; Tarasevich, B. J.; Campbell, A. A.; Fryxell, G. E.; Graff, G. L.; Song, L.; Liu, J.; Virden, J. W.; McVay, G. L. *Science* **1994**, *264*, 48−55.
(15) Küther, J.; Tremel, W. *Chem. Commun.* **1997**, *21*, 2029−2030.
(16) Aslam, M.; Sushama, P.; Bandyopadhyay, K.; Mulla, I. S.; Sainkar, S. R.; Mandale, A. B.; Vijayamohanan, K. *J. Mater. Chem.* **2000**, *10*, 1737−1743.
(17) DiBenedetto, S. A.; Facchetti, A.; Ratner, M. A.; Marks, T. J. *Adv. Mater.* **2009**, *21*, 1407−1433.
(18) Nitzan, A.; Ratner, M. A. *Science* **2003**, *300*, 1384.
(19) Yip, H.-L.; Hau, S. K.; Baek, N. S.; Ma, H.; Jen, A. K.-Y. *Adv. Mater.* **2008**, *20*, 2376−2382.
(20) Muthurasu, A.; Ganesh, V. *J. Colloid Interface Sci.* **2012**, *374*, 241−249.
(21) Kim, J. S.; Park, J. H.; Lee, J. H. *Appl. Phys. Lett.* **2007**, *91*, 112111.
(22) Sugimura, H.; Hozumi, A.; Kameyama, T.; Takai1, O. *Surf. Interface Anal.* **2002**, *34*, 550−554.
(23) Parikh, A. N.; Schivley, M. A.; Koo, E.; Seshadri, K.; Aurentz, D.; Mueller, K.; Allara, D. L. *J. Am. Chem. Soc.* **1997**, *119*, 3135−3143.
(24) William, A. *J. Am. Chem. Soc.* **1964**, *43*, 1−51.
(25) Golas, A.; Parhi, P.; Dimachkie, Z. O.; Siedlecki, C. A.; Vogler, E. A. *Biomaterials* **2010**, *31*, 1068−1079.
(26) Miozzo, L.; Yassar, A.; Horowitz, G. *J. Mater. Chem.* **2010**, *13*, 2513−2538.
(27) Love, J. C.; Estroff, L. A.; Kriebel, J. K.; Nuzzo, R. G.; Whitesides, G. M. *Chem. Rev.* **2005**, *105*, 1103−1169.
(28) Ma, H.; Yip, H. L.; Huang, F.; Jen, A. K.-Y. *Adv. Funct. Mater.* **2010**, *20*, 1371−1388.
(29) Chen, M. C.; Liaw, D. J.; Chen, W. H.; Huang, Y. C.; Sharma, J.; Tai, Y. *Appl. Phys. Lett.* **2011**, *99*, No. 223305.
(30) Bubel, S.; Mechau, N.; Hahn, H.; Schmechel, R. *J. Appl. Phys.* **2010**, *108*, 124502.
(31) Thitima, R.; Patcharee, C.; Takashi, S.; Susumu, Y. *Solid-State Electron.* **2009**, *53*, 176−180.
(32) Jouane, Y.; Colis, S.; Schmerber, G.; Kern, P.; Dinia, A.; Heisera, T.; Chapuis, Y.-A. *J. Mater. Chem.* **2011**, *21*, 1953−1958.
(33) Venables, J. A.; Spiller, G. D. T.; Hanbucken, M. *Rep. Prog. Phys.* **1984**, *47*, 399−459.
(34) Kline, R. J.; McGehee, M. D.; Toney, M. F. *Nat. Mater.* **2006**, *5*, 222−228.
(35) Erb, T.; Zhokhavets, U.; Gobsch, G.; Raleva, S.; Stuhn, B.; Schilinsky, P.; Waldauf, C.; Brabec, C. J. *Adv. Funct. Mater.* **2005**, *15*, 1193.
(36) Zhokhavets, U.; Erb, T.; Gobsch, G.; Al-Ibrahim, M.; Ambacher, O. *Chem. Phys. Lett.* **2006**, *418*, 347−350.
(37) Liu, S. W.; Su, W. C.; Lee, C. C.; Lin, C. F.; Cheng, C. W.; Chou, C. C.; Lee, J. H.; Chen, C. T. *Sol. Energy Mater. Sol. Cells* **2013**, *109*, 280−287.
(38) Hau, S. K.; Yip, H. L.; Acton, O.; Baek, N. S.; Ma, H.; Jen, A. *J. Mater. Chem.* **2008**, *18*, 5113−5119.